DEPARTMENT OF PHYSICS
Institute for Beam Physics and Technology

Stability Improvements at FLUTE
(Verbesserung der Stabilität von FLUTE)

Master thesis
of

Marvin-Dennis Noll

at the Institute for Beam Physics and Technology

Reviewer:	Prof. Dr.-Ing. John Jelonnek (IHM)
Second Reviewer:	Prof. Dr. Anke-Susanne Müller (IBPT)
Advisor:	Dr. Nigel Smale (IBPT)

15.11.2020 – 12.05.2021

Erklärung zur Selbstständigkeit

Ich versichere wahrheitsgemäß, die Arbeit selbstständig angefertigt, alle benutzten Hilfsmittel vollständig und genau angegeben und alles kenntlich gemacht zu haben, was aus Arbeiten anderer unverändert oder mit Abänderungen entnommen wurde und dass ich die Satzung des KIT zur Sicherung guter wissenschaftlicher Praxis in der gültigen Fassung vom 24.05.2018 beachtet habe.

Karlsruhe, den 10.05.2021, _____

Marvin-Dennis Noll

Als Prüfungsexemplar genehmigt von

Karlsruhe, den 10.05.2021, _____

Prof. Dr.-Ing. John Jelonnek (IHM)

Contents

List of Figures

List of Tables

Abstract

The **F**erninfrarot **L**inac- **U**nd **T**est-**E**xperiment (FLUTE), a compact linear accelerator, is currently designed and under commission at the Karlsruhe Institute of Technology (KIT). Its main purposes are to serve as a technology platform for accelerator research, the generation of strong and ultra short THz pulses and in the future as an injection device for **c**ompact **St**orage ring for **A**ccelerator **R**esearch and **T**echnology (cSTART).

At the current commissioning state, the klystron which powers the electron gun/RF cavity and in later stages the linear accelerator is fed by a pulse forming network, which is driven by a high voltage source connected to mains power. For high and a stable output power of the cavity resonator, several parameters have to be tuned to the correct values and kept inside of sometimes small tolerance bands.
In the past, the coolant temperature of the cavities water cooling system and the dependency of the pulse forming network output of the mains voltage phase were predominant sources of instability. After dealing with these issues, the cavity output power stability was improved significantly but further improvements to the stability were still desired.

In this work instead of passively optimizing the stability of system parameters, an active approach is evaluated. By controlling the amplitude of the RF input signal of klystron, which is easily possible since it is low power, the effects of noise and/or drifts are mitigated. Here it is evaluated if a simple of the shelf voltage controllable attenuator is a feasible choice to control the RF input signal, which input data should be used and which algorithm and/or control system is suitable to determine the needed attenuator setting to stabilize RF output (of the cavity).
Furthermore since the next stage in the system depends on a stable electron bunch charge rather than cavity power, it is determined whether the charge measurements of a Faraday cup can be used to directly control electron bunch charge.

Kurzfassung

–TODO–

1. Introduction

1.1. FLUTE - Ferninfrarot Linac- und Test-Experiment

2. Theoretical Background

3. Problem and Previous Work

4. Machine Diagnostics and Sensors

Most signals to be useful for diagnostics are available in EPICS. Retrieving their current value is therefore straight forward.

For example using the command line tool `caget` the last value of a PV can be obtained independent of the programming language used, however a syscall is needed which comes with a (slight) overhead and is inconvenient to use.

At least for Python and C++ there are EPICS libraries directly providing useful EPICS commands. A Python example of how to get the current cavity power is shown in Listing 4.1.

Listing 4.1: Get an EPICS PV with python

```
1 from epics import caget
2 cavity_power=caget("F:RF:LLRF:01:GunCav1:Power:Out")
```

4.1. Klystron and Cavity RF power

The RF power directly out of the klystron and right before the cavity are measured with TODO and available in EPICS.

4.2. Water Temperatures

Certain components of FLUTE that generate a lot of heat when in operation are water cooled. The cooling water temperatures are measured and delivered to EPICS.

4.3. Electron Bunch Charge

A faraday cup FARC-04[1] (by RadiaBeam Technologies) is used to measure the charge of an electron bunch.

At the moment it is read out with a PCB 421A25[2] charge amplifier. With the TODO-DAQ the output voltage signal ($\sim$ the charge) is fed into EPICS.

5. Influencing the LLRF with a RF Attenuator

A RF attenuator provides a fast and simple way of influencing the RF power delivery without interfering too much with existing subsystems, such as the LLRF MTCA system from DESY.

5.1. Requirements

In order for the attenuator to be useful for its application, some requirements are formulated first (Table 5.1).

Table 5.1.: Requirements against the attenuator is evaluated

Requirement	**Value**
attenuation set point resolution	0.1 dB
attenuation repeatability	0.01 dB
temperature range	TODO
voltage supply range	TODO

5.2. Selection and Overview of the selected Device

The ZX73-2500-S+ is a voltage controllable RF attenuator with coaxial SMA connectors by Mini-Circuits. As it is the only offering from Mini-Circuits of a RF attenuator with SMA connectors and is similar to devices from other manufactures, it is bought for evaluation.

Internally the ZX73-2500-S+ is based on the Mini Circuits RVA-2500+, a variable SMD attenuator in the DV874 case form factor. According to equivalent circuit in the data sheet in [3] it can be assumed it is based on the common quad-π pin diode design[4].

To get a first impression of the device capabilities, the attenuation over frequency measurements from the data sheet are repeated but with a higher maximum frequency of 4 GHz instead of 2.5 GHz (the highest frequency for which the attenuator is specified). Figure 5.1 shows the result.

In the next sections an operating point is chosen (only relative changes in attenuation are relevant) and then the influences of environment changes on the attenuation are examined.

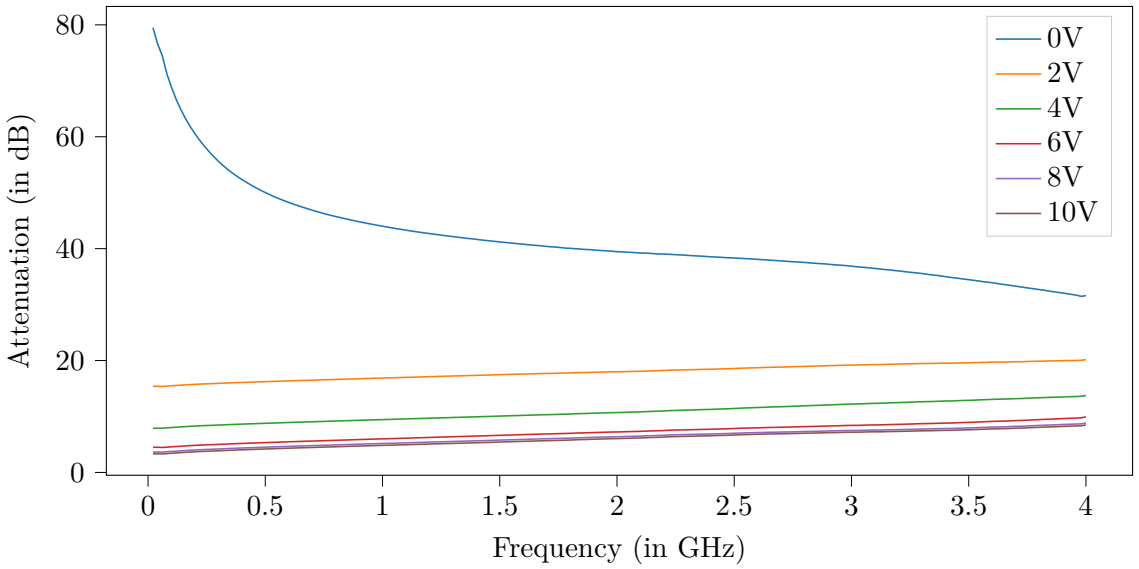

Figure 5.1.: Device attenuation vs. RF frequency over DC control voltage;
measured with network analyzer (see A.6.1, parameters: $\#AVG$: 16, $IF\text{-}BW$: 10 kHz)

5.3. Measurement setup

For all the following sections in this chapter,common measurement setup is needed. It needs to

- supply the attenuator with the supply voltage $V+$[1]
- feed in the (tunable) control voltage $V_{control}$
- supply RF power
- measure the attenuation
- keep track of $V+$, $V_{control}$ and the temperature ϑ_{case}

To achieve this, the setup in Figure 5.2 is used. In addition to the shown connection, each device is connected via Ethernet to a network switch and subsequently to a computer which runs a custom python program. Since all lab devices used are VXI11 compatible, they are easy to remote control. So for most measurements needed in this chapter no manual operation of the devices is needed and the program can set all parameters according to the test protocol before doing a measurement.

With the setup, a measurement frequency of about 0.5 Hz to 1 Hz can be achieved[2].

[1] To experiment with the influence of the supply voltage on attenuation, this also should be tunable.
[2] Limited by the long measurement times of the HP E4419B

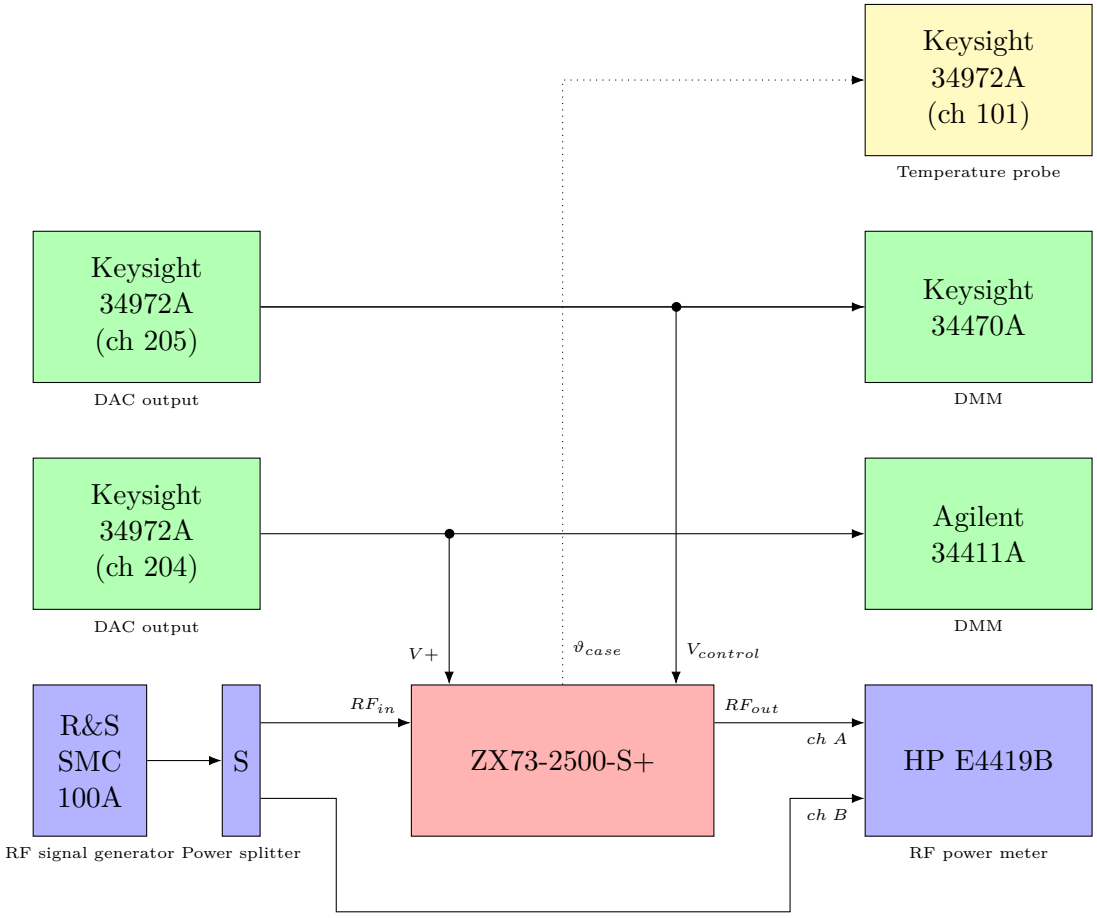

Figure 5.2.: Measurement setup: DUT(red), RF generator/power splitter/meter(blue), DC sources/meters(green), temperature probe(yellow)

5.4. Choosing an operating point

The spectra in Figure 5.1 already suggest that there is a nonlinear relation between the control voltage and the attenuation. This also implies a non-constant sensitivity. Therefore if a precise relative change in attenuation is desired, the needed change in the control voltage is not the same over the whole range of possible control voltages. Since the expected changes in attenuation (a few 0.1 dB) are small compared to the whole dynamic range of the device of about 80 dB, only small changes in the control voltage $V_{control}$ are necessary.

For the whole attenuator setup to meet the requirements in Table 5.1, the minimum changes in the control voltage needed by the devices operating point, need to be larger than any noise and instability of the control voltage source.

In Figure 5.3 the relation between attenuation A and the control voltage $V_{control}$ at a fixed RF frequency of 3 GHz is plotted. In addition, on the secondary axis, the sensitivity, with

$$\text{Sensitivity} :- \frac{\mathrm{d}A(V_{control})}{\mathrm{d}V_{control}} \tag{5.1}$$

is plotted, too.

The figure shows, that for low control voltages both the absolute attenuation is quite large and the magnitude of the sensitivity is also high. Operating the attenuator in this region would require a very stable control voltage (for example at $V_{control} = 2\,\mathrm{V}$, the sensitivity is $-10\,\frac{\mathrm{dB}}{\mathrm{V}}$).

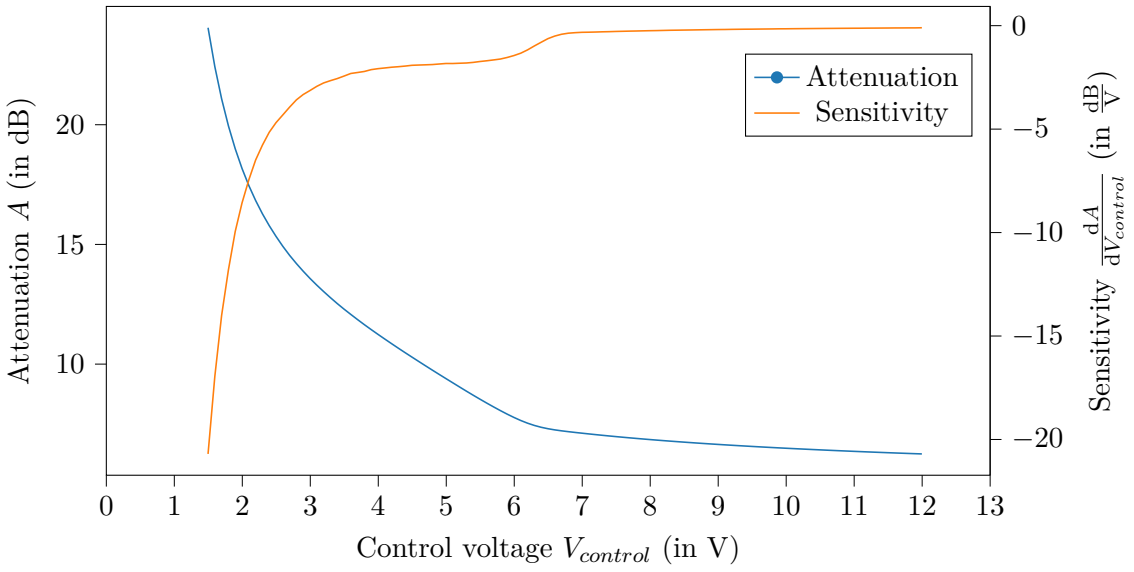

Figure 5.3.: Attenuation over control voltage

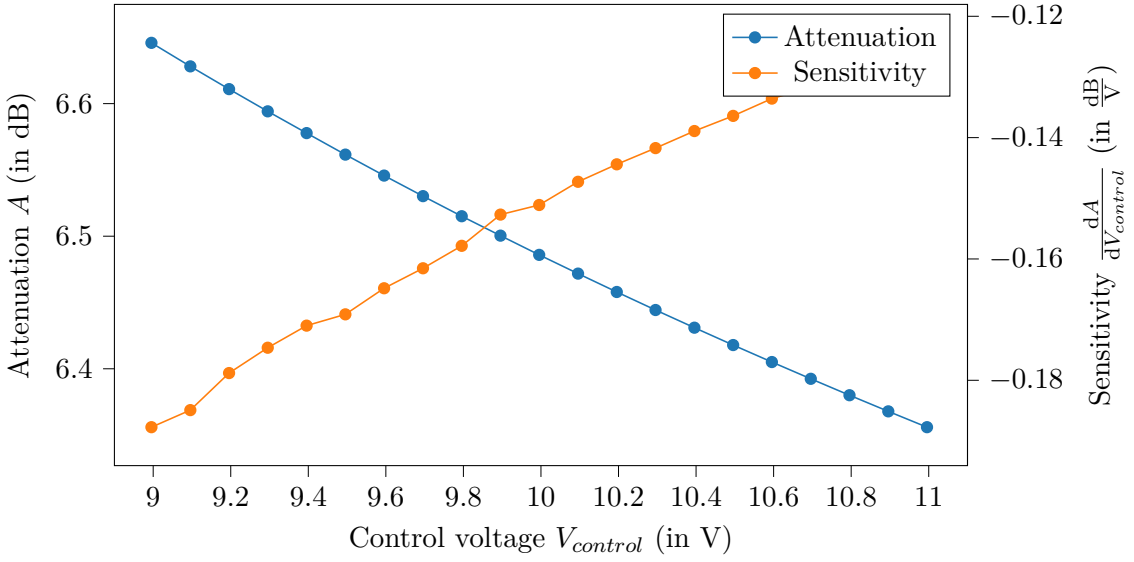

Figure 5.4.: Attenuation over control voltage (zoomed in version of Figure 5.3)

In Figure 5.4, the range $V_{control} = 10\,\mathrm{V} \pm 1\,\mathrm{V}$ is examined further. 10 V is chosen because the monotonically decreasing magnitude of the sensitivity suggests a high value but the maximum output voltage of the Keysight 34972A DAC of 12 V limits the choice. With 10 V there is still a margin for further experiments.

For now, the operating point is set to $V_{control} = 10\,\mathrm{V}$. For this control voltage, the absolute attenuation is $A = 6.48\,\mathrm{dB}$ and the sensitivity is $-0.1511\,\frac{\mathrm{dB}}{\mathrm{V}}$.

5.5. Stability requirements and measurement of the actual stability of $V_{control}$

5.5.1. Required stability

Figure 5.4 shows the attenuation A to be almost linearly dependent of $V_{control}$ in the vicinity of the operating point $V_{control,o} = 10\,\mathrm{V}$, thus the function $A(V_{control})$ can be approximated by its first order derivative around $V_{control,o}$:

$$A(V_{control}) - A(V_{control,o}) = \left.\frac{\mathrm{d}A(V_{control})}{\mathrm{d}V_{control}}\right|_o \cdot (V_{control} - V_{control,o}) \tag{5.2}$$

$$\Delta A(V_{control}) = \left.\frac{\mathrm{d}A(V_{control})}{\mathrm{d}V_{control}}\right|_o \cdot \Delta V_{control} \tag{5.3}$$

With $\left.\frac{\mathrm{d}A(V_{control})}{\mathrm{d}V_{control}}\right|_o = -0.1511\,\frac{\mathrm{dB}}{\mathrm{V}}$ and the required $\Delta A < 0.01\,\mathrm{dB}$ (so $\Delta A < 0.005\,\mathrm{dB}$ in one direction), the allowed deviation of $V_{control}$ from $V_{control,o}$, i.e. $\Delta V_{control}$ becomes

$$|\Delta V_{control}| = |\Delta A(V_{control})| \cdot \left| \left[\left.\frac{\mathrm{d}A(V_{control})}{\mathrm{d}V_{control}}\right|_o \right]^{-1} \right| \tag{5.4}$$

$$= 0.005\,\mathrm{dB} \cdot 6.618\,\frac{\mathrm{V}}{\mathrm{dB}} = 33.09\,\mathrm{mV} \tag{5.5}$$

Equation 5.4 requires the control voltage to be stable in the interval of $\pm 33\,\mathrm{mV}$ around the operating point.

5.5.2. Actual stability - long term

To asses the actual stability of $V_{control}$, delivered from the Keysight 34972A (see subsubsection A.2.1) DAC, first its long term stability over the course of one day is measured. For that the voltage is taken once every 2 seconds with a Keysight 34470A multimeter (see subsubsection A.1.2). The result is shown in Figure 5.5.

This measurement shows the stability of $V_{control}$ to be

$$\sigma_{V,control,longterm} = 0.173\,\mathrm{mV} \tag{5.6}$$

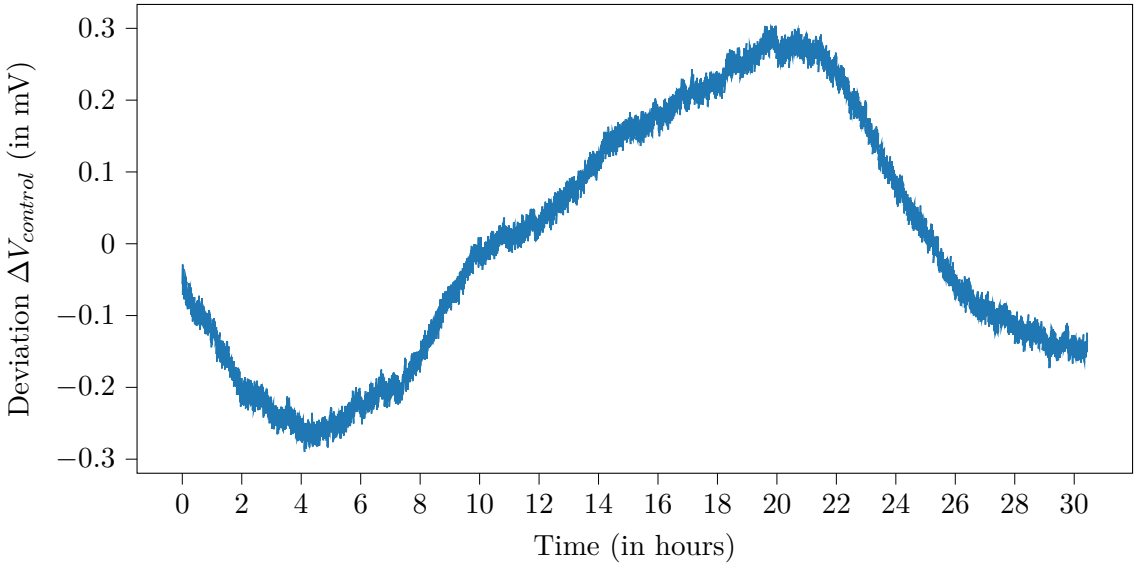

Figure 5.5.: Long term stability of $V_{control}$ as delivered by the Keysight 34972A DAC (ch. 205); measured with Keysight 34470A;
room temperature during measurement: $\mu_\vartheta = 19.12\,°\text{C}$, $\sigma_\vartheta = 0.28\,°\text{C}$

5.5.3. Actual stability - short term

Since the Keysight 34470A has a limited bandwidth of 15 kHz, higher frequency noise is not captured in Figure 5.5. Therefore for short term stability the DAC channel is measured again with a Tektronix MSO64 oscilloscope (subsubsection A.3.1,on the 500 MHz bandwidth setting). The resulting time signal is shown in Figure 5.6, the spectrum shows Figure 5.7.

This measurement shows the stability of $V_{control}$ to be

$$\sigma_{V,control,shortterm} = 7\,\text{mV} \tag{5.7}$$

5.5.4. Conclusion

With an allowed deviation of 33 mV, the output resolution of the Keysight 34972A DAC ($^{24\,\text{V}}/_{2^{16}-1} = 366.22\,\mu\text{V}$) and its stability (0.173 mV long term, 7 mV short term) pose no problems on the device operation (if the other parameters are to be assumed with no error).

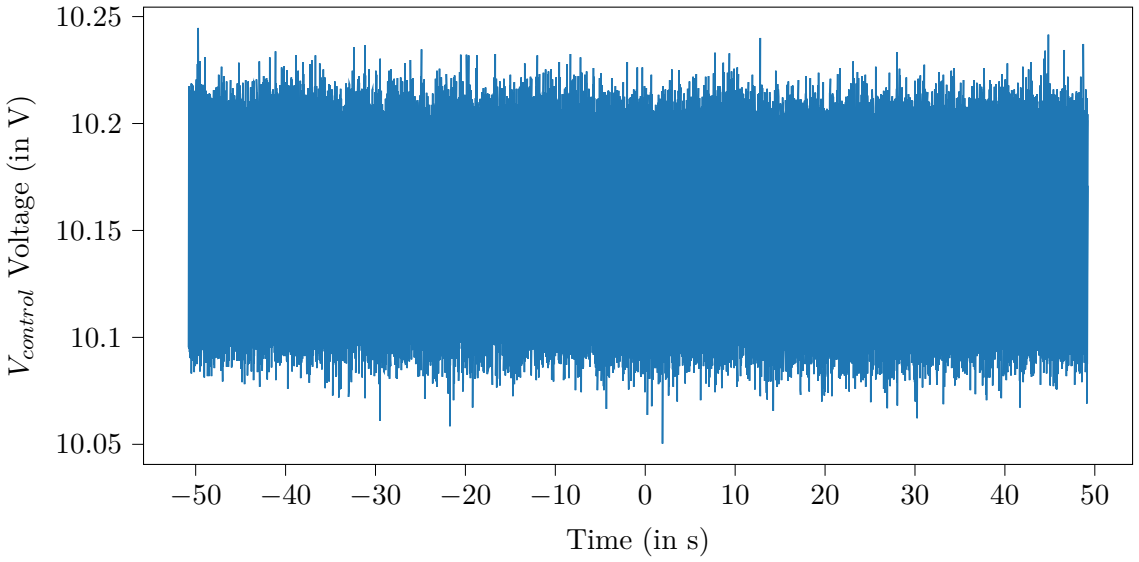

Figure 5.6.: Short term stability of $V_{control}$ as delivered by the Keysight 34972A DAC (ch. 205); measured with Tektronix MSO64

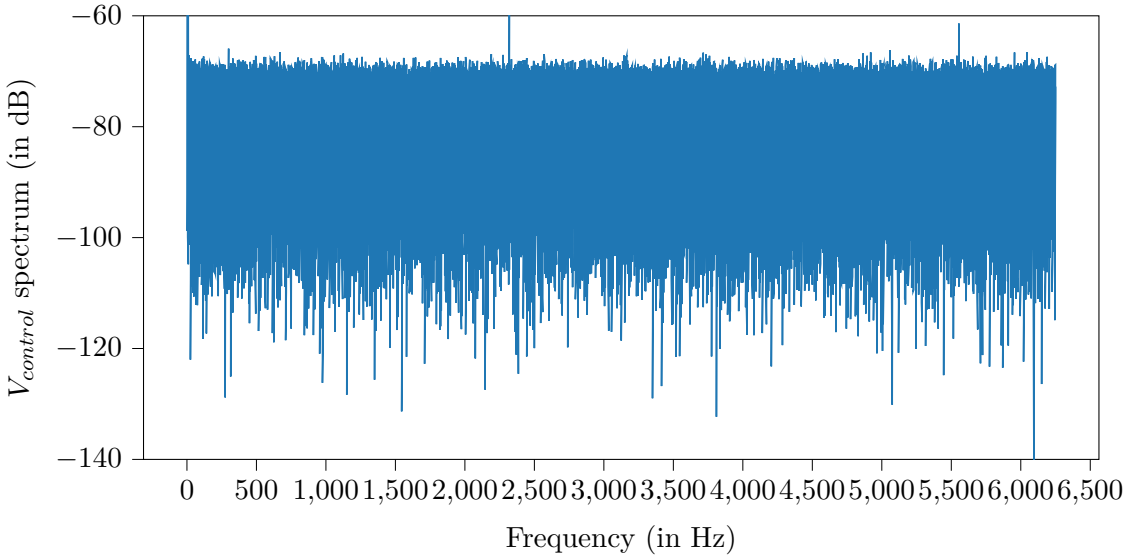

Figure 5.7.: Power spectrum of $V_{control}$

5.6. Stability requirements and measurement of the actual stability of V_+

5.6.1. Required stability

To get the required stability for the power supply voltage, the effect of the power supply voltage $V+$ on the attenuation has to be examined first. For that $V+$ is varied $\pm 0.2\,\mathrm{V}$ around the nominal supply voltage of $V+_0 = 3\,\mathrm{V}$, all other parameters are kept constant and the attenuation is measured. To make the measurement more robust against fluctuations of the room temperature and drift of the devices, the procedure of stepping through the voltages is repeated and the means for each set $V+$ are computed. The result is shown in Figure 5.8.

This leads to:

$$\Delta A(V+) = \left.\frac{\mathrm{d}A(V+)}{\mathrm{d}V+}\right|_o \cdot \Delta V+ \tag{5.8}$$

$$\Delta A(V+) = 0.003\,75\,\frac{\mathrm{dB}}{\mathrm{V}} \cdot \Delta V+ \tag{5.9}$$

which means the allowed deviation of $V+$ from $V+_0$ becomes

$$|\Delta V_+| = |\Delta A(V+)| \cdot \left| \left[\left.\frac{\mathrm{d}A(V_+)}{\mathrm{d}V_+}\right|_0 \right]^{-1} \right| \tag{5.10}$$

$$= 0.005\,\mathrm{dB} \cdot 266.67\,\frac{\mathrm{V}}{\mathrm{dB}} = 1.33\,\mathrm{V} \tag{5.11}$$

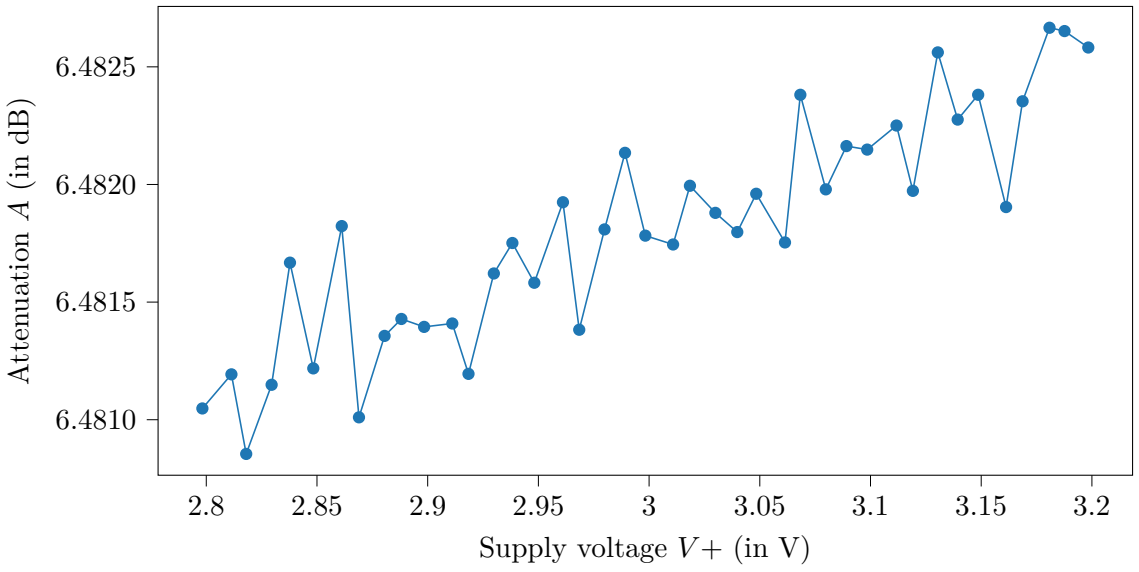

Figure 5.8.: Influence of the supply voltage on the attenuation

5.6.2. Actual stability - long term

This long term measurement yields a standard deviation of

$$\sigma_{V,+,longterm} = 0.154\,\mathrm{mV} \tag{5.12}$$

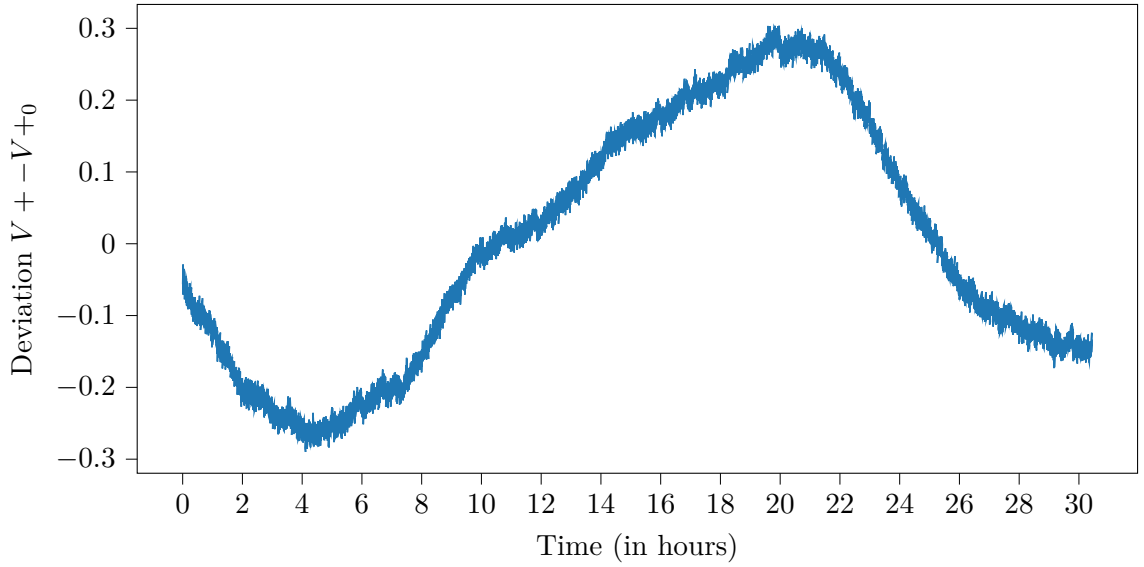

Figure 5.9.: Long term stability of $V+$ as delivered by the Keysight 34972A DAC (ch. 204); measured with Keysight 34470A;
room temperature during measurement: $\mu_\vartheta = 19.12\,°\mathrm{C}$, $\sigma_\vartheta = 0.28\,°\mathrm{C}$

5.6.3. Actual stability - short term

Again because of the lower bandwidth of the multimeter compared with an oscilloscope (compare subsection 5.5.3), the short term stability is evaluated with an oscilloscope measurement (see Figure 5.10 and Figure 5.11).

The oscilloscope measurement shows a much higher standard deviation than the multimeter measurement of

$$\sigma_{V,+,shortterm} = 50\,\mathrm{mV} \tag{5.13}$$

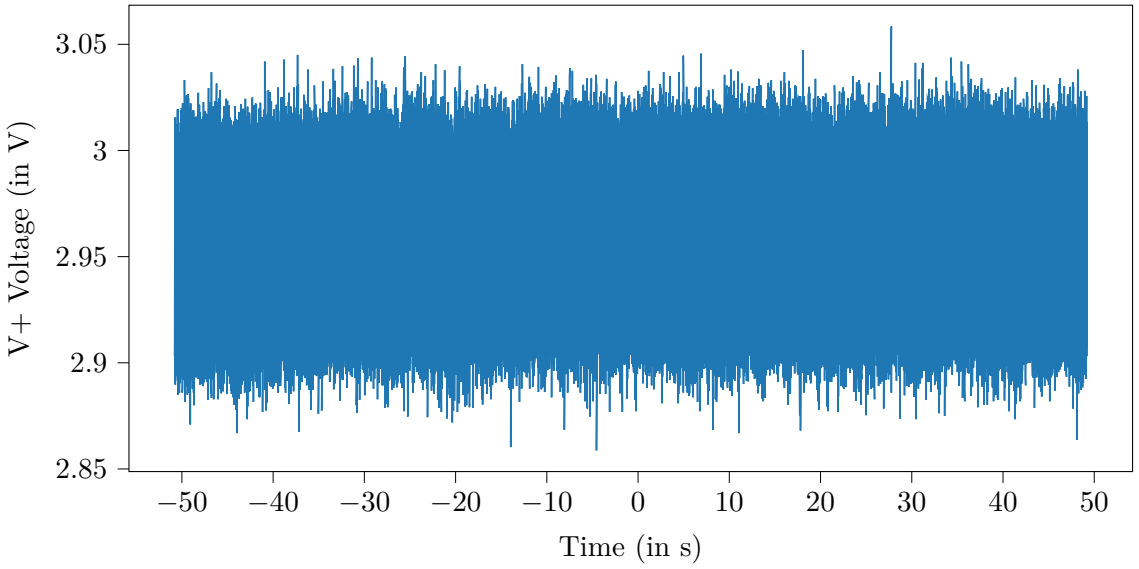

Figure 5.10.: Short term stability of $V+$ as delivered by the Keysight 34972A DAC (ch. 204); measured with Tektronix MSO64

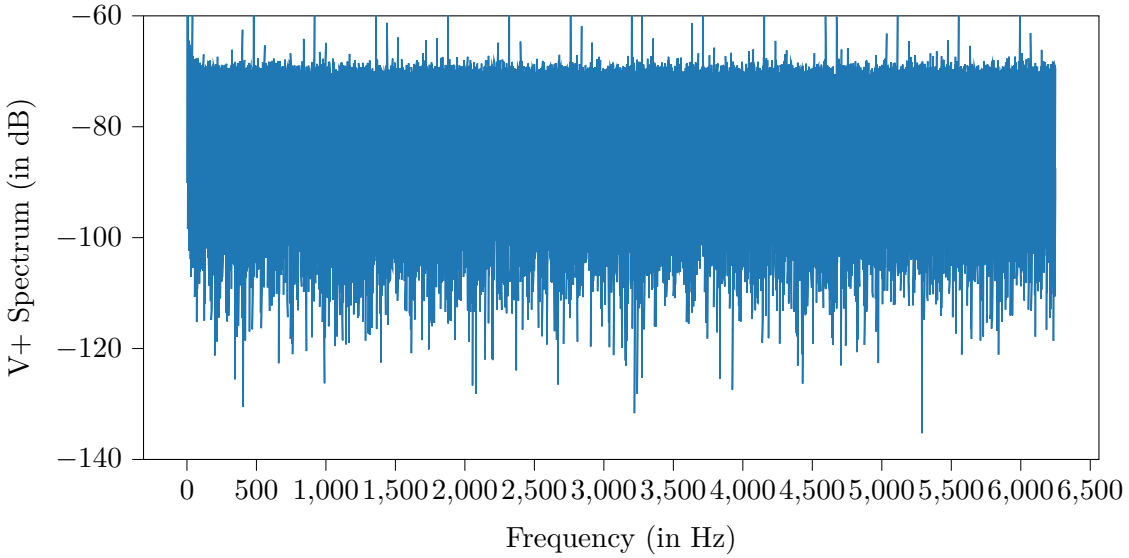

Figure 5.11.: Power spectrum of $V+$

5.6.4. Conclusion

The short term noise with $\sigma_{V,+,shortterm} = 50\,\mathrm{mV}$ is fairly high compared to the other DAC channel (with a higher output voltage). But these variations are not visible on the multimeter due to the lower bandwidth ($\sigma_{V,+,longterm} = 0.154\,\mathrm{mV}$). This suggests the power supply can simply be stabilized with a RC lowpass or just a capacitor at the devices supply voltage input.

But even without compensation the effects of the high frequency noise could not be seen in the attenuation, so device naturally rejects high frequency noise on its supply input.

5.7. Stability requirements of the case temperature θ_{case}

5.7.1. Required stability

To asses acceptable temperature change, first the influence of the device temperature of the attenuation is measured. For that the bottom of the device is fixed to a rectangular iron profile with zip ties. The iron profile is heated with the tip of a soldering iron (set to 150 °C) for 1 min and then allowed to cool for 20 min. This cycle is repeated three times and the device temperature and the attenuation are measured once every 2 s. Due to the dynamic flow of heat from the soldering iron to the iron profile and through device itself, a strong hysteresis is visible in the curve in Figure 5.12.

To linearly approximate the temperature influence, the single measurements are binned together for similar temperature values (rounded to two decimal places). Then a mean operation is applied over the binned values (see Figure 5.13).

From that the slope of the curve is taken at $\vartheta_{case,0} = 23\,^{\circ}\mathrm{C}$[3].

With a slope of $\left.\frac{\mathrm{d}A(\vartheta_{case})}{\mathrm{d}\vartheta_{case}}\right|_0 = 0.0075\,\frac{\mathrm{dB}}{\mathrm{K}}$, the influence on attenuation becomes

$$\Delta A(\vartheta_{case}) = \left.\frac{\mathrm{d}A(V_{control})}{\mathrm{d}V_{control}}\right|_o \cdot \Delta T_{case} \tag{5.14}$$

$$\Delta A(\vartheta_{case}) = 0.0075\,\frac{\mathrm{dB}}{\mathrm{K}} \cdot \Delta V+ \tag{5.15}$$

which means the allowed deviation of ϑ_{case} from $\vartheta_{case,0}$ becomes

$$|\Delta\vartheta_{case}| = |\Delta A(\vartheta_{case})| \cdot \left| \left[\left.\frac{\mathrm{d}A(\vartheta_{case})}{\mathrm{d}\vartheta_{case}}\right|_0 \right]^{-1} \right| \tag{5.16}$$

$$= 0.005\,\mathrm{dB} \cdot 133.33\,\frac{\mathrm{K}}{\mathrm{dB}} = 0.666\,\mathrm{K} \tag{5.17}$$

This would even be hard to achieve in climatized office spaces (like the IBPT RF lab), since aird conditioners can only keep the room temperature stable to about 2 °C (depending on the distance to the air outlet, other heat sources in the room, open windows, etc.).

[3] This is not necessarily room temperature or expected operating temperature of the device but a convenient choice to get a linear curve section.

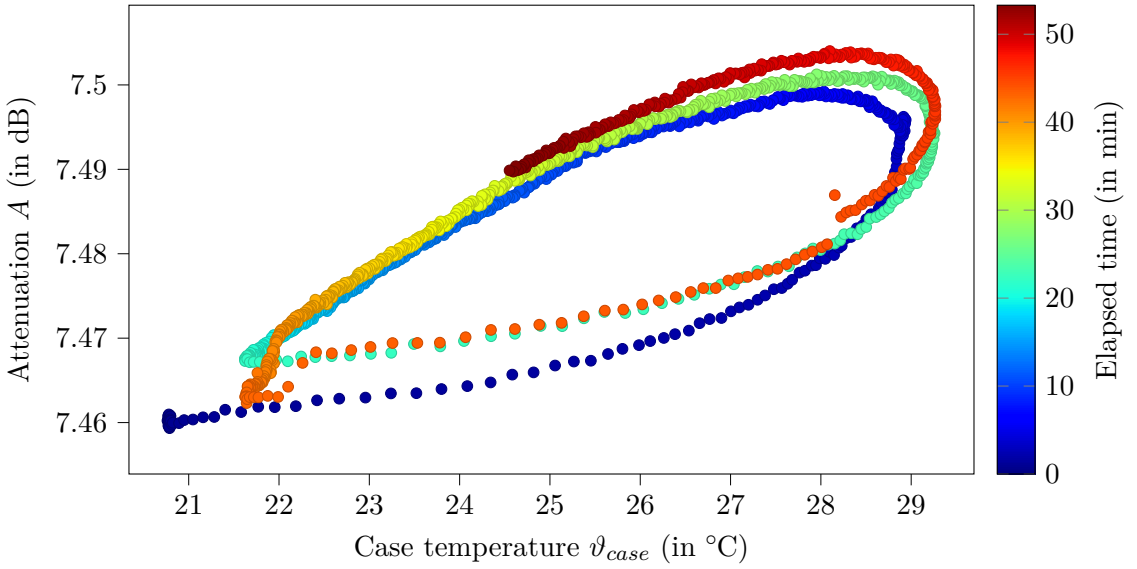

Figure 5.12.: Attenuation over case temperature; color scale shows time progress of the total measurement

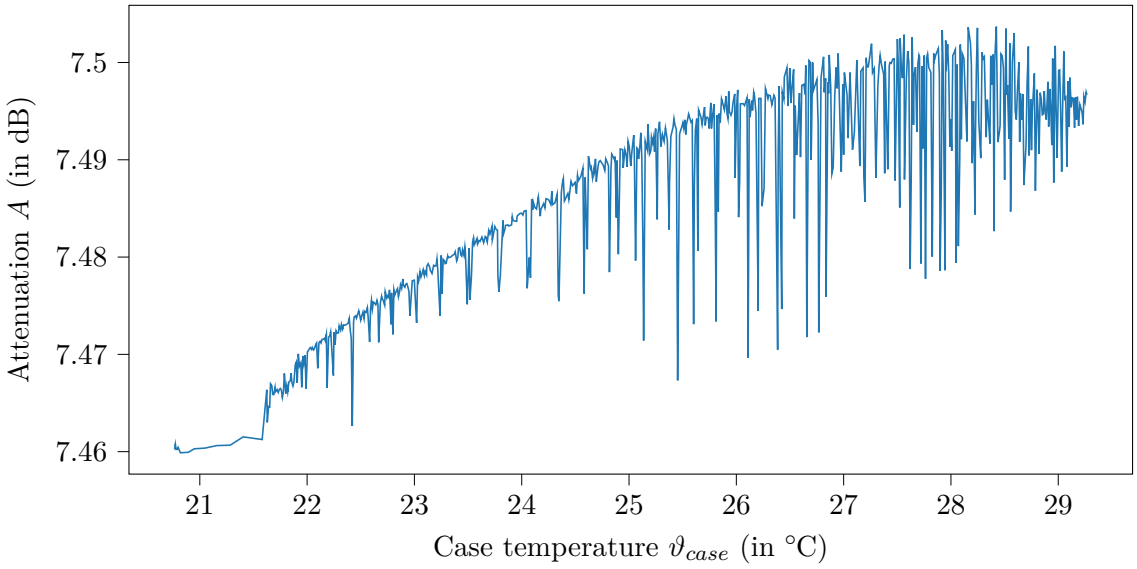

Figure 5.13.: Attenuation over case temperature

5.7.2. Conclusion

The results in Figure 5.13 and Equation 5.16 suggest two solutions:

- Either mount the device in a temperature controlled cabinet to keep the temperature constant.
- Or since the plot in Figure 5.13 shows the slope becoming more flat towards higher temperatures, it could may be possible to operate the device on purpose at higher case temperatures (According to the data sheet[3], the maximum operating temperature is 85 °C).

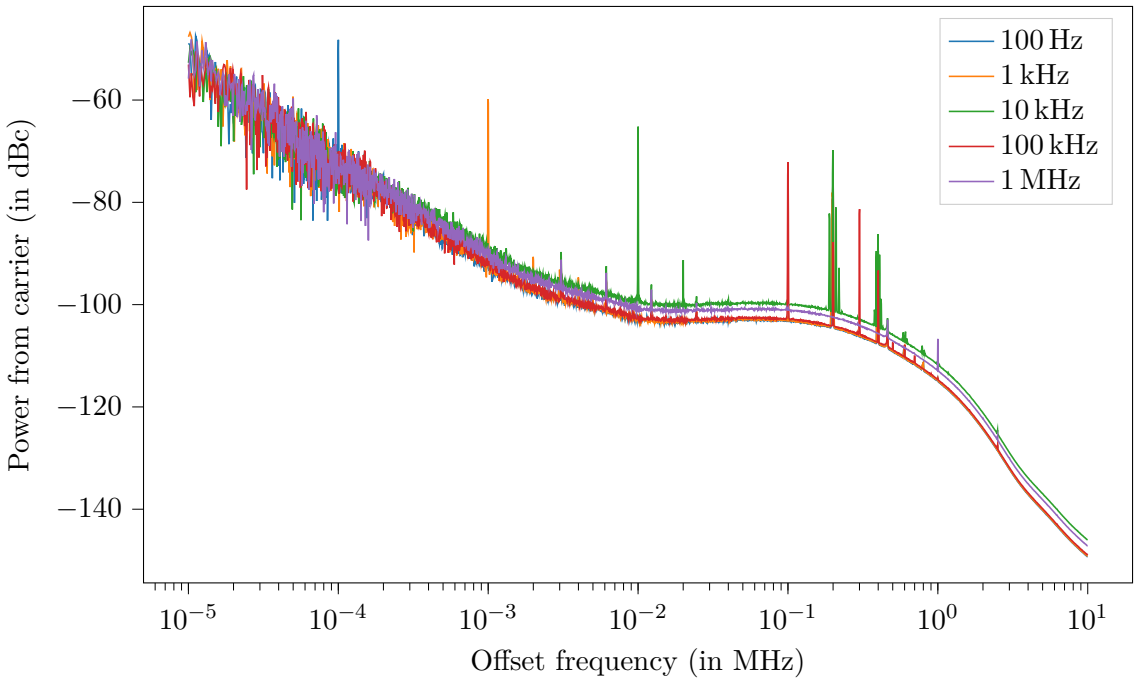

Figure 5.14.: Spectrum (measured with Holzworth HA7062A (subsubsection A.7.1)) showing the effect of modulating $V_{control}$ with different frequencies (Modulation amplitude: 1 V)

5.8. $V_{control}$ Frequency response

Using a non inverting adder with a *TS912IN* operational amplifier, a sine wave with constant offset is made, which is then used to drive the control voltage $V_{control}$. The result for different sine wave frequencies is shown in Figure 5.14.

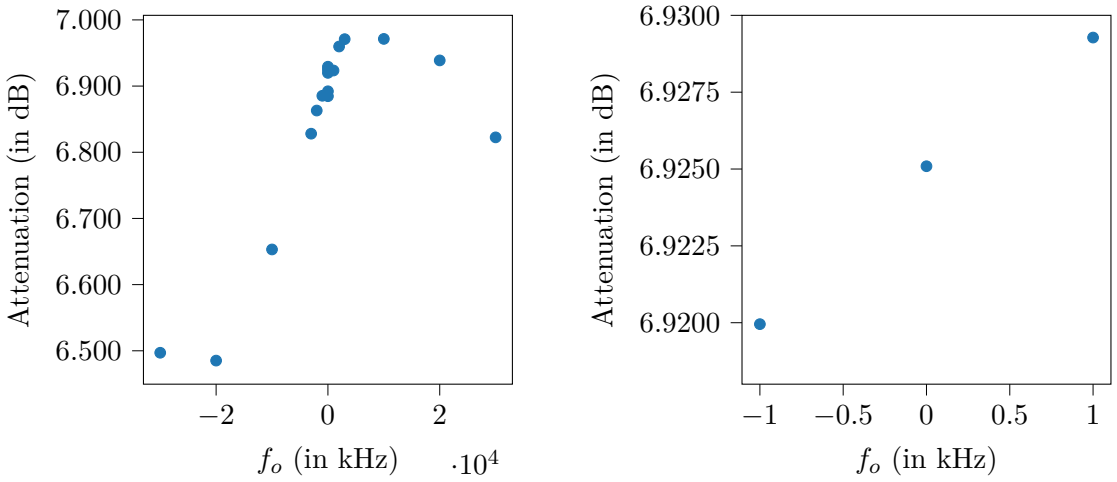

(a) $f_o = \pm 30\,\text{kHz}$ **(b)** $f_o = \pm 1\,\text{kHz}$

Figure 5.15.: Attenuation vs. offset frequency $f_o = f - 3\,\text{GHz}$

5.9. Influence of RF frequency variations

In this section the influence of a varying RF frequency on attenuation is examined. For that the set frequency of the R&S SMC100 signal generator is varied while the attenuation is measured with the HP E4419B RF power meter. The result is shown in Figure 5.15.

5.10. Testing the Attenuator in the RF cabinet at FLUTE

Without FLUTE being switched on, the attenuator is left in the RF cabinet in the bunker basement. Over the course of 100 h, the case temperature is taken every two seconds and the deviation from the mean temperature 25.4 °C is computed (see Figure 5.16). The figure also shows a power spectrum (calculated using Welch's method with a hanning window) of the temperature deviation.

With a standard deviation of 0.055 22 K, a maximum positive swing of 0.18 K and a maximum negative swing of 0.17 K (a span of 0.3559 K), the temperature stability is well inside the 0.6 K tolerance.

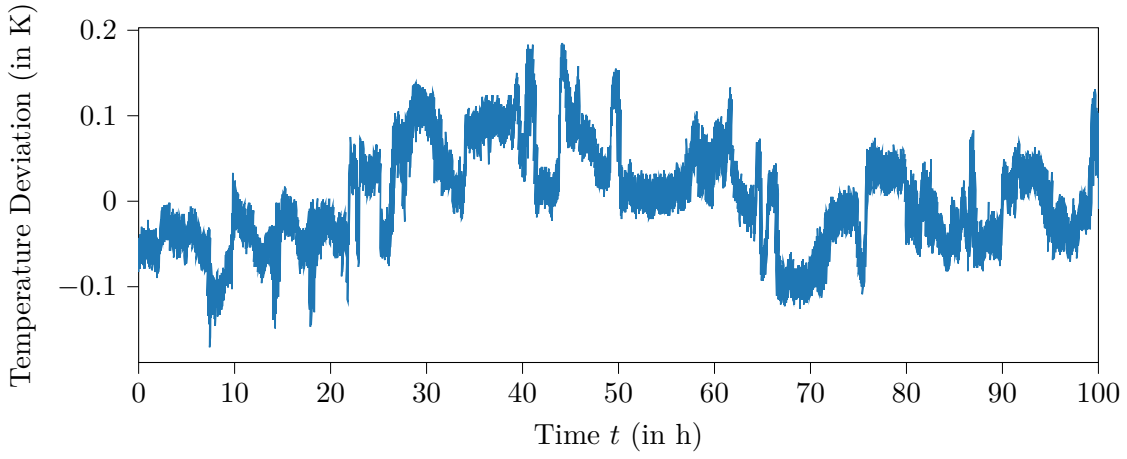

(a) Time

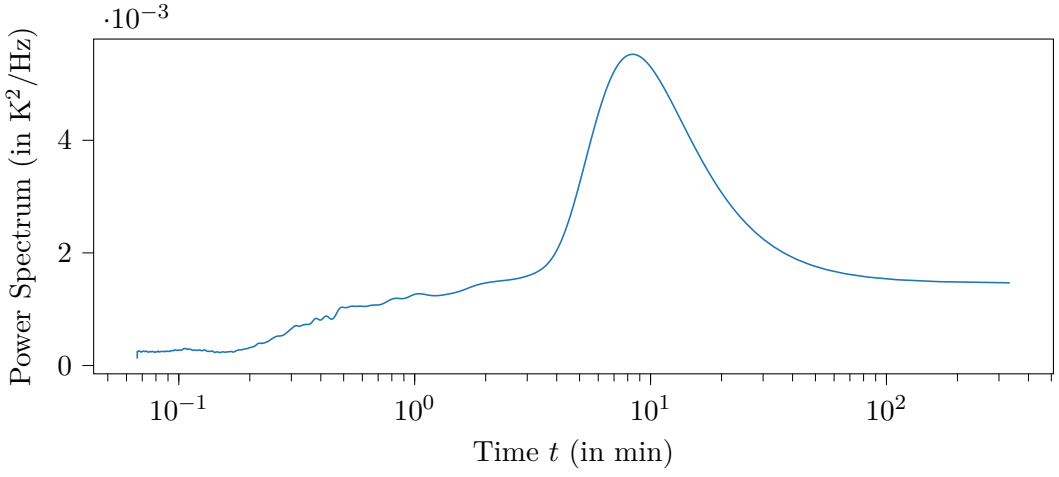

(b) Spectrum with peak at around 8 min

Figure 5.16.: Temperature of the attenuator inside the RF cabinet without a load

6. Implementing a Feedback Control System

In this chapter stabilizing the power output of FLUTE by means of a control system is examined. This is different than previous attempts in that a feedback control system tries to compensate short term disturbances and long term drifts *actively* by interfering with some part of FLUTE that has influence of the output power.

The next sections describe the chosen architecture of a suitable control system as well as some implementation details and the tuning of necessary controller parameters.

6.1. Architecture

The general structure of a closed loop control system is shown in Figure 6.1.

$y(t)$ is the physical quantity which should follow a certain time trajectory $x(t)$ or be kept constant (then $x(t) = x = const.$). If there are no disturbances $d(t)$ or the disturbances are deterministic (i.e. $d(t)$ is known $\forall t$), then an open loop system would be possible. In that case the role of the controller would be to merely to set its output $u(t)$ according to the system dynamics of the plant[1] (represented by its impulse response $g(t)$).

In most real world scenarios, $d(t)$ originates from a stochastic process and thus is unknown. Too remedy the negative influences of $d(t)$, the output $y(t)$ is measured and feed back. Based on the error $e(t)$, which is the difference between the set value and the actual value defined by

$$e(t) = x(t) - y(t), \tag{6.1}$$

the controller can react accordingly.

[1] Assuming $g(t)$ is a stable LTI system

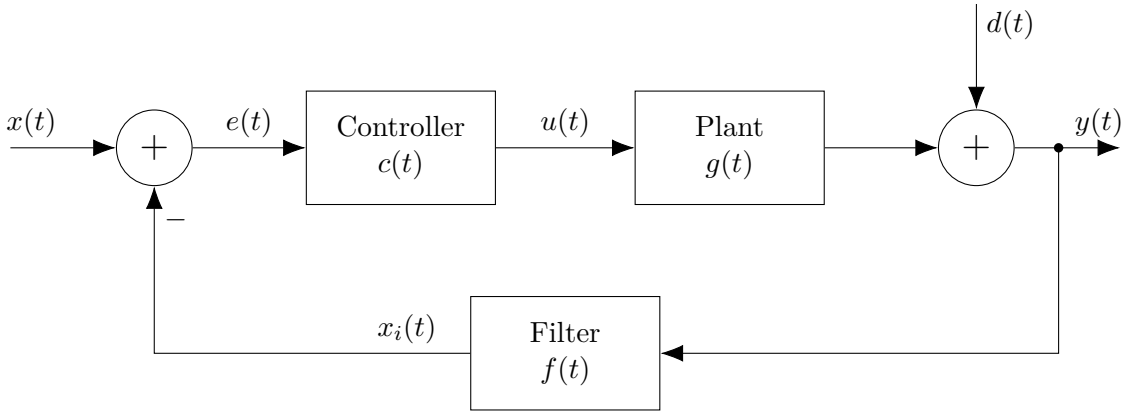

Figure 6.1.: General structure of a closed loop feedback control system

6.2. Inputs and Outputs

Since the control algorithm should be implemented, tested and used online on the actual accelerator instead of only operate on simulated data, there is the need for fast and reliable interfaces to the machine. Following, "input'' refers to the signal going into the control algorithm (i.e. the measured $y(t)$), while "output'' is the output of the control algorithm $u(t)$.

6.2.1. Input

Depending on which value is chosen to be controlled, filtering of the input signal could be mandatory.

In the case of the cavity RF power the signal jumps to zero each time a breakdown occurs, shortening the RF supply. These outliners are not representative of the average RF power inside the cavity over multiple pulses and thus would greatly impair the controller performance. For that reason, before any further filtering to remove noise etc, a breakdown removal filter is used (Listing 6.1). In principle the new power value is checked to be inside a band which size is determined by the mean deviation of the N_{filt} previous values and a scaling m. The percentile differences are used here as they are robust against outliners (i.e. other breakdowns) in the N_{filt} previous values opposed to a normal standard deviation. The scaling with $(2 * 1.2815)^{-1}$ is used to make the mean deviation comparable to a standard deviation.

Listing 6.1: Breakdown removal

```
#...
if(abs(P[i]-np.median(P[i-3*Nfilt:i-Nfilt]))<
m*(np.percentile(P[i-3*Nfilt:i-Nfilt],90)-np.percentile(P[i-3*Nfilt:i-Nfilt],10)/(2*1.2815))):
    P_filt =np.append(P_filt,P[i])
else:
    breakdown_locations_predicted=np.append(breakdown_locations_predicted,i)
    P_filt =np.append(P_filt,np.median(P[i-3*Nfilt:i-Nfilt]))
#...
```

6.2.2. Output

For the control system to work the controller needs some way of influencing the plant. For that the output of the FLUTE LLRF vector modulator is controlled by a RF attenuator (see chapter 5).

6.3. Plant Identification

6.3.1. Principle

Before choosing an appropriate controller, some insight of the system response has to be obtained. For that reason, next the plant transfer function is obtained. In the time domain, the transfer function is the response of the system to an impulse on the input. So per definition, in the special case here, this would mean changing the RF attenuator quickly from a big attenuation to a small attenuation and then back. This is not easy to measure and a single measurement is very susceptible to noise. Therefore it is more common to measure the step response instead and to average over several step responses.

When there is no prior knowledge over the system, the identification is sometimes done with a (pseudo) random binary sequence to excite the system with step functions of different lengths. Then it is necessary that some of the steps last longer than a few dominant time constants of the system. To get the transfer function of the system from its step response, several methods are common, including correlation based and frequency response based algorithms.

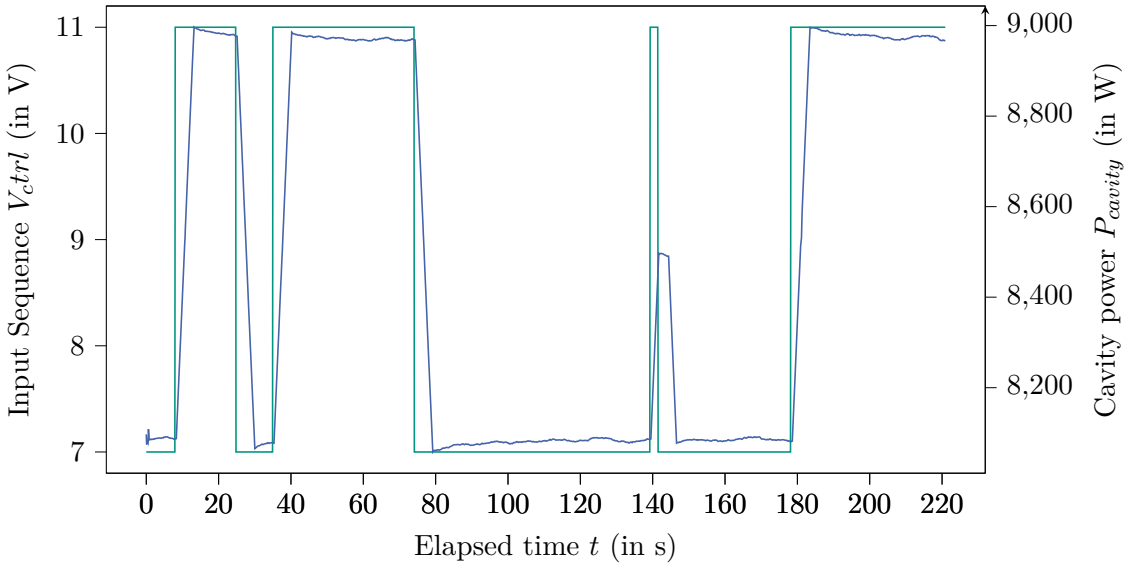

Figure 6.2.: Small section of the input sequence (green) and the system response (blue)

6.3.2. Identifying the system response of the FLUTE LLRF

The input sequence is generated by modulating the RF attenuator around a base attenuation. As a trade off between high SNR and driving the LLRF in a "save" region, the control voltage span is chosen to be 4 V in total (7 V to 11 V around the base control voltage of 9 V).

To get a random binary sequence, depending on the outcome of a binomial random process, the voltage is toggled between 7 V and 11 V according to Listing 6.2. With the parameter `toggleP`, the average length of one constant voltage level can be controlled.

Listing 6.2: Function to get a random binary sequence

```
1 def randomBinarySequence(N,toggleP):
2     u=[False]*N
3     for i in range(1,len(u)):
4         if(np.random.binomial(1,toggleP,1)[0]):
5             u[i]=not u[i-1]
6         else:
7             u[i]=u[i-1]
8     return list(map(lambda x: 7 if x==False else 11,u))
```

In a test run over 6 hours (after FLUTE had stabilized), the attenuator was driven with such a random sequence. The result is shown in Figure 6.2.

The time signals are then split into a estimation data set (about 80 % of samples) and a validation data set (the remaining ≈ 20 %).

The two data sets are then loaded into the MATLAB *System Identification Toolbox* (SIT). With the SIT, first the means of both sets and both the input and output are removed, which is required by the estimators used. Then with different numbers of poles and zeros, the transfer function is estimated. After trying several settings, three promising candidates

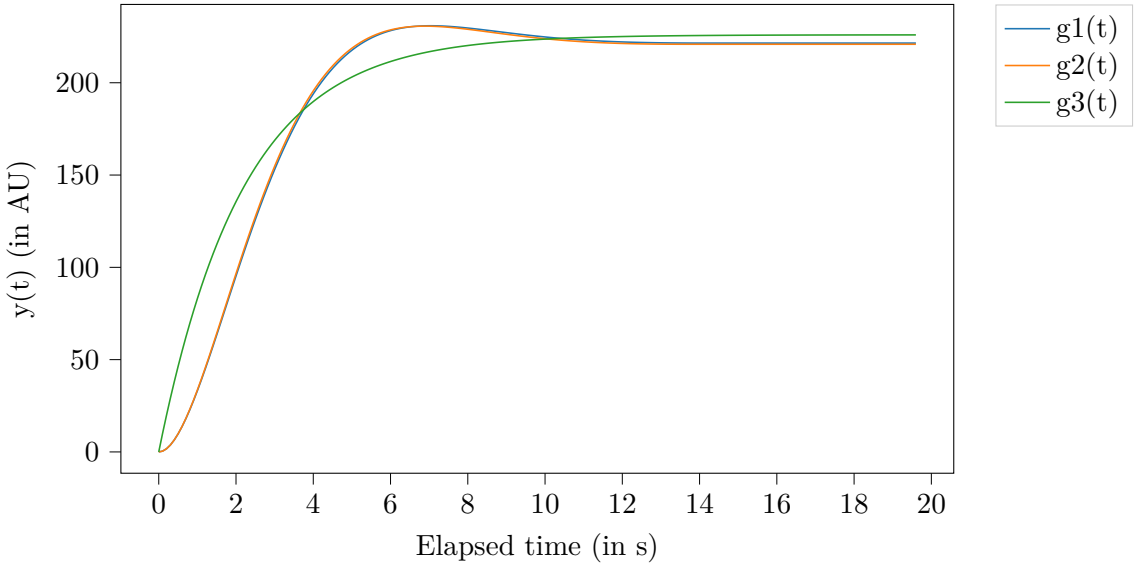

Figure 6.3.: Step responses of the systems $\hat{G}_1(s)$, $\hat{G}_2(s)$, $\hat{G}_3(s)$

$$\hat{G}_1(s) = \frac{71.37\,s + 0.5966}{s^3 + 0.8208\,s^2 + 0.328\,s + 0.002733} \tag{6.2}$$

$$\hat{G}_2(s) = \frac{-0.2125\,s + 70.85}{s^2 + 0.8022\,s + 0.3202} \tag{6.3}$$

$$\hat{G}_3(s) = \frac{79.12}{s + 0.3502} \tag{6.4}$$

emerge.

For these transfer functions, the (single) step responses are given in Figure 6.3.

To check the accuracy of the estimations, the SIT is used to do a simulation with the $\hat{G}_i(s)$ and the validation data set (see Figure 6.4).

Figure 6.4 shows that a first order system with one pole and no zeros is not a sufficient approximation as there is no overshoot, since it is not possible in a first order system. The second and third order systems $\hat{G}_2(s)$ and $\hat{G}_3(s)$ show much better fits.

The important conclusion of this section is that the plant can be modeled as a **second order system**. This info is needed when choosing a controller in the next section.

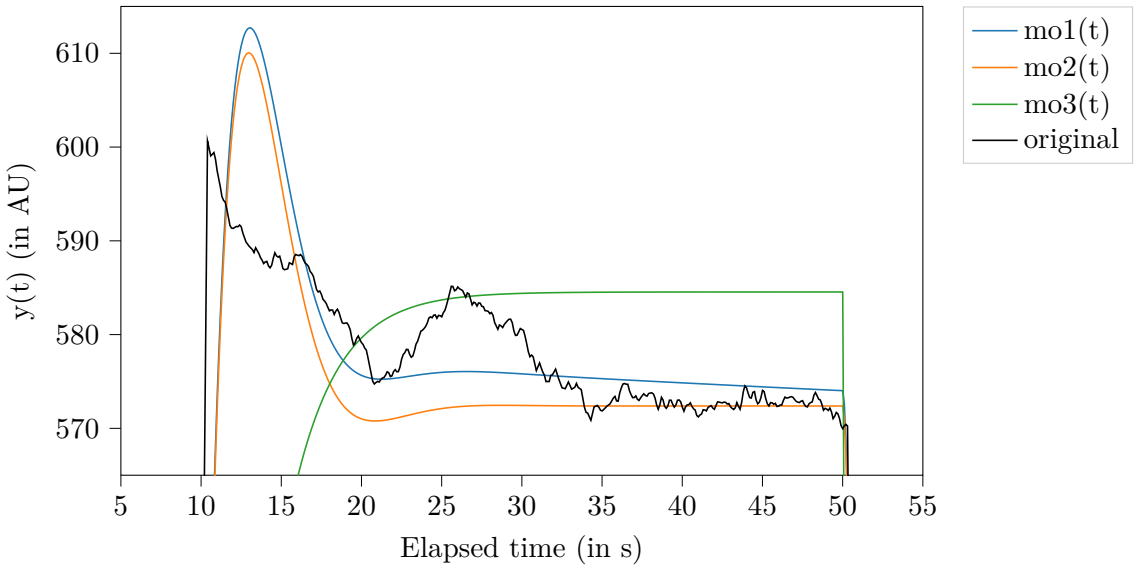

Figure 6.4.: Validating the estimations $\hat{G}_1(s)$, $\hat{G}_2(s)$, $\hat{G}_3(s)$ against real data from the validation data set

6.4. Controller design

For many control problems, especially if the plant behaves approximately as an LTI system and the system is of low order, a simple PID (proportional, integral and derivative) controller is a good starting point (visualized in Figure 6.5).

A PID controller uses the error $e(t)$, the temporal integral of the error $e_i(t)$ and the temporal derivative of the error $e_d(t)$ as an input and outputs a weighed sum of them. While the unmodified error signal represents the current error, the integrated and derived error signals allow to controller to "see" in the past and predict the future.

Often simplifications, such as a pure P (only $k_p \neq 0$) or a PI (only k_p, $k_i \neq 0$) controller are valid as well. Since the plant has been identified to be a second order system, a simple P controller is not enough to bring the steady state error to zero (see). So at least a PI controller is needed.

As a starting point for software development and parameter tuning, the parameters $k_p = 0.00001$ and $k_i = k_d = 0$ are chosen. This ensures during development the system basically does nothing but still shows changing values at the controller output.

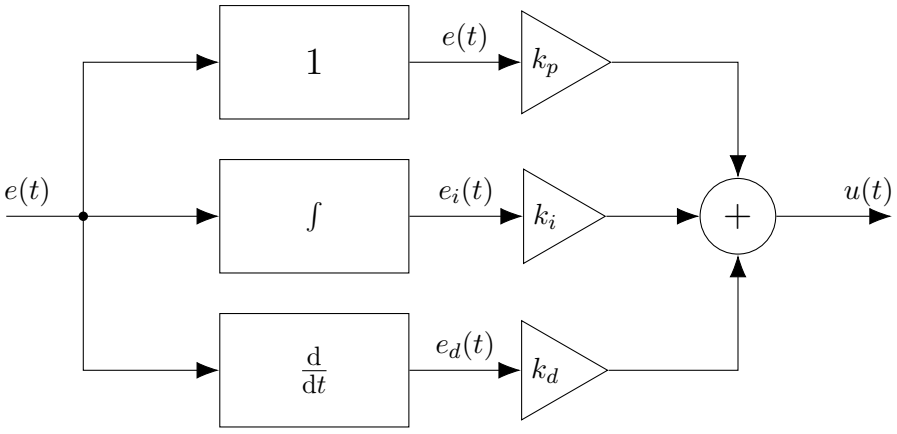

Figure 6.5.: Block diagram of a generic PID controller

6.5. Software Design

As integrating a new subsystem into EPICS takes some time and effort and the control system is designated a temporary solution, it is more viable to operate it as an independent system.

Before choosing a programming language, software frameworks, etc. the key requirements for the software are discussed:

- Communication with EPICS to get values and with the RF attenuator
- Efficient and lightweight to achieve clock cycles times of a most 0.1 s
- Easy implementation of a (time discrete) PID controller
- GUI to show input, output and error signals
- Possibility to log signals to file for documentation

With these in mind first programming languages are regarded. As there are EPICS libraries for both C++ and Python, these two languages are examined in more detail.
While C++ as a compile language promises speed, all other requirements are possible but would take much greater effort in C++ compared to Python. For that reason, in the following a small test program is written to evaluate the fastest clock cycle possible with a simple Python program.

shows that retrieving one value of an EPICS channel and setting a new attenuator voltage takes only about 20 ms, thus using C++ is not necessary and Python can be utilized instead.

To create a PID controller in software instead of a continuous time system, only discrete time implementations are possible. Choosing a high clock cycle frequency however approximates the continuous time system. To get the error signals for the integral and derivative part, the integral is replaced with a cumulative recursive sum as

$$e_i[n] = e_i[n-1] + e[n] \cdot dt, \tag{6.5}$$

while the derivative is replaced by a difference

$$e_d[n] = \frac{e_i[n-1] - e[n]}{dt}. \tag{6.6}$$

For the GUI a common framework should be used. In Python Tk and wxwidgets are common ways to build a GUI. Another viable option is PyQt, which, as the name suggests, is a Python port of the Qt framework. One major advantage of using PyQt is the possibility to import `.ui` files describing the GUI directly from the Qt RAD designer called "Qt designer'', removing the need to create the GUI programmatically. Furthermore using PyQt enables the usage of *pyqtgraph*, a highspeed plotting library only compatible with Qt. This ensures plotting live data does not bottleneck performance, which is often the problem with naive *matplotlib* based solutions.

To log all relevant data from RAM to non-volatile memory (hard drive or network share), a simple approach with a line by line CSV writer is used.

6.6. Control Parameter Tuning and Tests

To tune control parameters there are a multiple of analytical, empirical or hybrid approaches. Here the Ziegler-Nichols method is tested and fine tuning is done by hand.

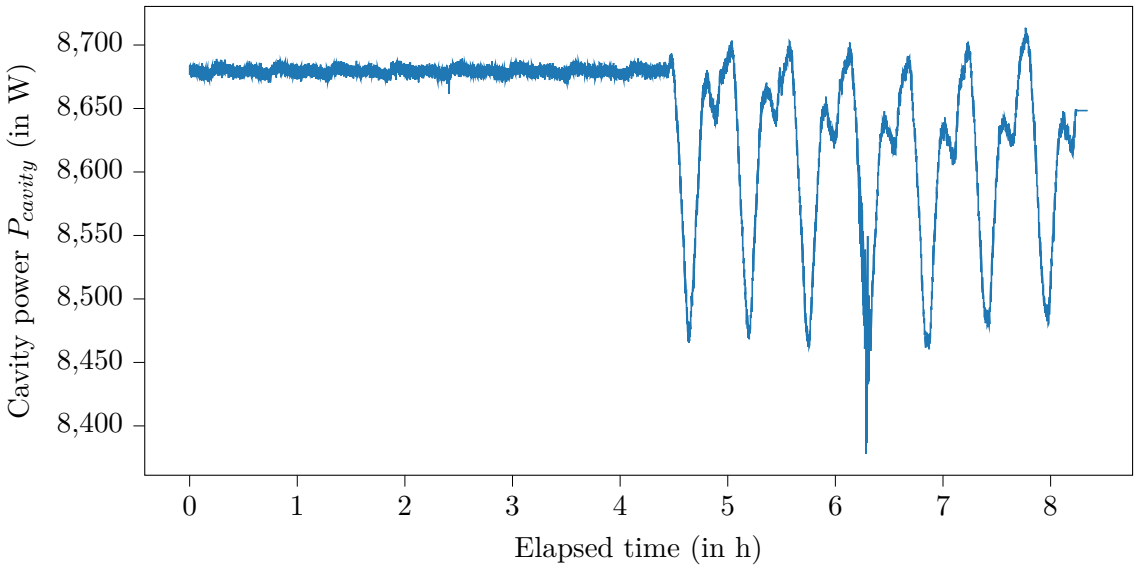

Figure 6.6.: Cavity power with PID controller on (before the 4.5 h mark) and off shows the stabilizing effect of the control system

6.7. Results

As Figure 6.6 shows, with the control system activated, the standard deviation drops from about 150 W to less than 10 W, which shows the effectiveness of the system.

6.8. Summary and Improvement Suggestions

7. Results

8. Conclusion and Outlook

8.1. Conclusion

8.2. Outlook

Appendix

A. Lab Test and Measurement Equipment

A.1. Benchtop multimeters

A.1.1. Agilent 34411A

Table A.1.: Agilent 34411A specifications

Specification	**Value**
	DC volt
Digits	6 1/2
Measurement method	cont integrating multi-slope IV A/D converter
Accuracy (10 V range, 24 hours)	0.0015 %+0.0004 % (% of reading + % of range)
Bandwidth	15 kHz (typ.)

Table A.2.: Agilent 34411A some SCPI commands

Description	**Example command**	**Example return**
Read current measurement	`READ?`	`+2.84829881E+00` (2.848 V)

A.1.2. Keysight 34470A

Table A.3.: Keysight 34470A specifications

Specification	**Value**
	DC volt
Digits	7 1/2
Measurement method	cont integrating multi-slope IV A/D converter
Accuracy (10 V range, 24 hours)	0.0008 %+0.0002 % (% of reading + % of range)
Bandwidth (10 V range)	15 kHz (typ.)

Table A.4.: Keysight 34470A some SCPI commands

Description	**Example command**	**Example return**
Read current measurement	`READ?`	`+9.99710196E+00` (9.997 V)

A.2. Data Acquisition/Switch Unit

A.2.1. Keysight 34972A

Table A.5.: Keysight 34972A specifications

Specification	Value
34907A (Multifunction module)	
DAC range	±12 V
DAC resolution	16 bit ($^{24\,V}/_{2^{16}} = 366.21\,\mu V$ per bit)
DAC maximum current	10 mA
34901A (20 channel multiplexer)	

Table A.6.: Keysight 34972A some SCPI commands

Description	Example command	Example return
Read current measurement	`READ?`	`+2.00200000E+01` (20.02 °C)
Set DAC voltage of ch 204 to 3.1 V	`SOUR:VOLT 3.1,(@204)`	

A.3. Oscilloscopes

A.3.1. Tektronix MSO64

Table A.7.: Tektronix MSO64 specifications

Specification	Value
Bandwidth	6 GHz
Sample rate	25 GS/s
ADC resolution	12 bit
DC gain accuracy (@ 50 Ω, >2 mV/div)	±2 %

Table A.8.: Tektronix MSO64 some SCPI commands

Description	Example command	Example return
Read mean of measurement 1 (current acq.)	`MEASUrement:MEAS1:RESUlts:CURR:MEAN?`	`3.0685821787408`

A.4. RF signal generator

A.4.1. Rohde and Schwarz SMC100A

Table A.9.: Rohde and Schwarz SMC100A specifications

Specification	Value
Frequency range	9 kHz to 3.2 GHz
Maximum power level	17 dBm
SSB phase noise (@ 1 GHz, $f_o = 20$ kHz, $BW = 1$ Hz)	−111 dBc
Level error	<0.9 dB

Table A.10.: Rohde and Schwarz SMC100A some SCPI commands

Description	Example command	Example return
Set RF power level to 10.5 dBm	`SOUR:POW 10.5`	
Set RF frequency to 3.1 GHz	`SOUR:FREQ:FIX 3.1e9`	
Enable the RF output	`OUTP on`	

A.5. RF power meter

A.5.1. HP E4419B

Table A.11.: HP E4419B specifications

Specification	Value
Digits	4
Accuracy (abs. without power sensor)	±0.02 dB
Power probe: E4412A	
Frequency range	10 MHz to 18 GHz
Power range	−70 dBm to 20 dBm

Table A.12.: HP E4419B some SCPI commands

Description	Example command	Example return
Measure power on input 1	`MEAS1?`	`+2.89435802E+000` (2.894 dBm)

A.6. Vector Network Analyzer

A.6.1. Agilent E5071C

Table A.13.: Agilent E5071C specifications

Specification	Value
Frequency range	9 kHz to 8.5 GHz

A.7. Phase noise analyzer

A.7.1. Holzworth HA7062C

Table A.14.: Holzworth HA7062C specifications

Specification	Value
DUT input frequency	10 MHz to 6 GHz
Measurement bandwidth	0.1 Hz to 40 MHz offsets

Bibliography

[1] RadiaBeam, *Faraday Cups*. [Online]. Available: `http://www.radiabeam.com/upload/catalog/pdf/14272334342015-03-24_faraday-cups.pdf`.

[2] P. Synotech, *PCB 421A25 Charge Amplifier*.

[3] Mini-Circuits, *ZX73-2500+ Voltage Variable Attenuator*.

[4] R. W. Waugh, "A Low-Cost Surface Mount PIN Diode π Attenuator'', vol. 35, no. 5, pp. 280–284, 1992.